C_{60} on the Pt(111) surface: Structural tuning of electronic properties

X. Q. Shi,[1] A. B. Pang,[2] K. L. Man,[2] R. Q. Zhang,[1] C. Minot,[1,3] M. S. Altman,[2] and M. A. Van Hove[1]

[1]*Department of Physics and Materials Science, City University of Hong Kong, Hong Kong, China*

[2]*Department of Physics, The Hong Kong University of Science and Technology, Hong Kong, China*

[3]*Laboratoire de Chimie Théorique, Unité Mixte de Recherche No. 7616 associée au Centre National de la Recherche Scientifique, Université Pierre & Marie Curie, Case Postale 137, 4 place Jussieu, F-75252 Paris Cedex 06, France*

(Received 25 August 2011; published 1 December 2011)

The structure and electronic properties of the $(\sqrt{13} \times \sqrt{13})R13.9^\circ$ and $(2\sqrt{3} \times 2\sqrt{3})R30^\circ$ ordered phases of C_{60} on the Pt(111) surface are investigated using combined dynamic low-energy electron diffraction and density functional theory (DFT) calculations. The two phases have the same local adsorption structure, while they are predicted by DFT calculations to exhibit very different electronic structures due to their different inter-C_{60} orientations and distances. This result demonstrates the structural tuning of electronic properties for molecular films or junctions composed of the same materials.

DOI: 10.1103/PhysRevB.84.235406 PACS number(s): 68.35.bp, 68.37.Ef, 71.15.Nc, 73.20.At

I. INTRODUCTION

Carbon-60 films on metal surfaces are of great interest due to their rich structural and electronic properties, their potential use in molecular electronics, and their importance in understanding the principles underlying organic-metal interactions. A wide range of electronic band structures has been reported for C_{60} monolayers.[1–3] The band structures strongly depend on the structural details such as the interface reconstruction[4] and the relative C_{60} orientations, the latter being due to the high angular momentum of the C_{60} molecular orbitals.[5,6] To make use of these unique electronic properties, it is therefore important to understand and to gain control over the C_{60}-metal and inter-C_{60} degrees of freedom.

Usually, C_{60} molecules adsorbed on metal surfaces form hexagonal or nearly hexagonal structures in various orientations with a molecular center-to-center distance of at least ~9.5 Å.[7–11] Adsorption can induce charge transfer between C_{60} and substrate and can modify the molecules' structural and electronic properties as well.[4] On Pt(111), C_{60} forms two distinct phases, labeled $(\sqrt{13} \times \sqrt{13})R13.9^\circ$ and $(2\sqrt{3} \times 2\sqrt{3})R30^\circ$ (hereafter referred to as the $\sqrt{13}$ and $2\sqrt{3}$ phases, respectively; note that $2\sqrt{3} = \sqrt{12}$ is just 4% smaller than $\sqrt{13}$, so the $2\sqrt{3}$ phase is slightly compressed relative to the $\sqrt{13}$ phase; in terms of unit-cell areas and thus density, the compression is $1 - 12/13 \sim 8\%$).[12,13] These two phases have different intermolecular orientations and distances, as will be demonstrated in the following. Therefore, one may expect the two phases to exhibit different electronic properties. In earlier work, while the $\sqrt{13}$ phase was found to occur alone, the $2\sqrt{3}$ phase was reported to occur only in coexistence with the $\sqrt{13}$ phase. This makes it difficult to detect and exploit the potentially different electronic properties of the two phases.[2,3,13] In our work, however, we have found it possible to isolate the two phases.

Carbon-60 forms strong covalent bonds with Pt on Pt(111);[14] adsorbed C_{60} on Pt(111) also allows metal wave functions to propagate further out from the metal.[15] These properties can lead to an extremely high conductivity of C_{60} contacts with Pt electrodes.[16] Although the electronic and transport properties reported for C_{60}/Pt(111) are exceptional and the electronic properties of the two structural phases can be anticipated to be different, there appear to have been no reports of the electronic properties for C_{60} in either of the two possible single-phase structures on Pt(111).[13] Structural studies of these systems are also incomplete. The structure of the $\sqrt{13}$ phase has been determined with x-ray diffraction[14] to involve the presence of a vacancy below the C_{60} molecule. Such reconstructions are expected to be the rule rather than the exception in C_{60} adsorption on metals.[7] Similar structures for C_{60} on Pt(111) were proposed based on scanning tunneling microscopy observations,[12] but have not been confirmed by any direct method.

In this work, we first obtain uniform monolayers of the pure $\sqrt{13}$ and $2\sqrt{3}$ structural phases of C_{60} on Pt(111) through careful control of the deposition and annealing temperatures. The adsorption geometries are then determined by combined dynamic low-energy electron diffraction (LEED) analysis and density functional theory (DFT) calculations. We find that the local adsorption geometry is the same in the two structures. In particular, reconstruction of the Pt(111) surface involving single-atom vacancy formation is a common feature of the two adsorption geometries. Based on the determined structures, significant differences in the electronic structures for C_{60} monolayers in these two phases are predicted by DFT calculations, which we believe can be attributed mainly to the relative rotation of neighboring C_{60} molecules.

II. METHOD

The Pt(111) sample was cleaned by repeated cycles of Ar-ion bombardment at 1.5 kV and annealing to 1150 K, with occasional annealing cycles in O_2 at pressure $P = 2 \times 10^{-7}$ Torr at 1000 K to remove carbon contamination. The sample temperature was measured using a type-*C* thermocouple attached to the sample holder at the edge of the Pt sample. Carbon-60 was deposited at a rate of 0.1 ML/min from a Mo crucible in an electron-beam heated deposition source. The pure $\sqrt{13}$ phase was produced here by depositing 1.4 ML of C_{60} at 300 K followed by annealing to 500 K for 20 min. The $\sqrt{13}$ diffraction intensities were stable following desorption of C_{60} in excess of 1 ML during annealing. We found that annealing at slightly higher temperature, 550 K, caused the $\sqrt{13}$ diffraction intensities to decrease steadily

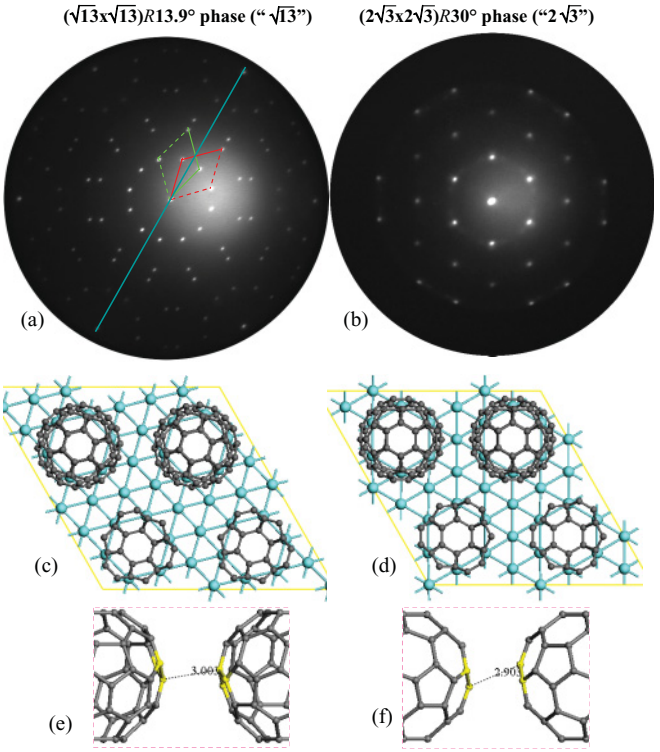

FIG. 1. (Color online) LEED patterns of C_{60}/Pt(111) in (a) the $(\sqrt{13} \times \sqrt{13})R13.9^\circ$ phase (at 37.2 eV) and (b) the $(2\sqrt{3} \times 2\sqrt{3})R30^\circ$ phase (at 15.3 eV). Also shown are the corresponding real-space supercells (doubled in both directions for ease of viewing) of the final determined structures in the (c) $\sqrt{13}$ and (d) $2\sqrt{3}$ phases, respectively [C (Pt) atoms are colored gray (blue)]. To display the C_{60}/Pt interface clearly, the lower C_{60} molecules include only their bottom part; each C_{60} sits above a Pt vacancy. Panels (e) and (f) show the inter-C_{60} face-to-face contacts viewed parallel to the surface. In (a), green and red rhombi denote two symmetrically equivalent mirrored domains and the blue line indicates the mirror plane; in (c), only one of the two mirrored domains is shown (while mirroring leaves the $2\sqrt{3}$ structure invariant).

during annealing, possibly due to the onset of fragmentation.[13] The pure $2\sqrt{3}$ phase was produced without any trace of the $\sqrt{13}$ phase by depositing C_{60} directly at 500 K followed by postannealing at the deposition temperature for 20 min. The $2\sqrt{3}$ diffraction intensities increased steadily during deposition at this elevated temperature and reached a plateau when the monolayer was complete. Growth beyond 1 ML coverage at 500 K was inhibited by the low sticking probability of C_{60} on the complete monolayer. The LEED intensity-voltage (I-V) curves were measured in a low-energy electron microscope operated in diffraction mode, corresponding to normal incidence.[17] The experimental data presented in Fig. 2 were obtained with the sample held at 83 K. Measurements that were carried out at 300 K produced almost identical results, except for strong suppression of diffraction intensities above about 150 eV due to the Debye-Waller effect.

Low-energy electron diffraction patterns for the $\sqrt{13}$ and $2\sqrt{3}$ phases are shown in Figs. 1(a) and 1(b). The $\sqrt{13}$ LEED pattern has two equivalent mirrored domains and each domain shows threefold rotational symmetry. The $2\sqrt{3}$ LEED pattern shows threefold symmetry and a mirror plane. The I-V curves are extracted for each spot and the symmetrically equivalent spots are averaged, which results in a total data set having a cumulative energy range of 4860 eV for the $\sqrt{13}$ phase and 3080 eV for the $2\sqrt{3}$ phase. The widest energy range for one spot goes from 150 to 733 eV. The lower energies (below 150 eV) are not used in the intensity analysis because they are less sensitive to the C_{60}/metal interface structure, which is buried about 7 Å below the external surface [similarly, Ref. 7, for C_{60} on Ag(111), also adopted a higher-energy range]. The LEED calculations use our SATLEED package.[18] The agreement between the experiment and theory is quantified by the Pendry R factor. The phase shifts (with $l_{max} = 9$) are calculated from the superposition of atomic potentials with optimized muffin-tin radii, as tested previously.[19,20] The DFT calculations use the VASP package[21] in the local density approximation,[22] which was shown to be able to describe both the energetic and electronic properties of C_{60} on metal surfaces.[1,2,7,9,23] Projector augmented wave potentials are used[24] and the cutoff energy is 400 eV. The other calculation details are the same as those in Ref. 23. To find the best-fit structures, first DFT calculations were performed for many possible structures and then LEED calculations were performed for the more promising DFT structures (assuming threefold symmetry). The adsorption sites considered were unreconstructed atop, hollow (hcp and fcc), and bridge, on top of a single-atom Pt vacancy and on top of a seven-atom Pt vacancy [the latter is the preferred geometry of C_{60} on Cu(111) (Ref. 4)]. At each site, different rotations of C_{60} around the surface normal were considered, with a hexagonal face pointing down to suit the observed symmetry.[12]

III. RESULTS AND DISCUSSION

The final determined structures are displayed in Figs. 1(c) and 1(e) and in Figs. 1(d) and 1(f). Typical experimental and calculated LEED I-V spectra for the optimized structure are shown in Fig. 2. Tables I and II indicate that both DFT and LEED give the same conclusion, namely, that the single-atom vacancy adsorption structure is the most stable and fits the LEED data best for both phases. The R factors are comparable to the similar systems C_{60}/Ag(111) (Ref. 7) and C_{60}/Cu(111) with a larger data set.[4] As Table III exhibits, DFT and LEED agree closely, the two phases have almost identical local adsorption structures, and they show a strong covalent C-Pt bond character.[14] These results agree with the model

TABLE I. Adsorption energies per cell (the $2\sqrt{3}$ and $\sqrt{13}$ cells have different areas) for the most favored unreconstructed and reconstructed (one- and seven-atom hole) structures (in eV): The one-atom hole structure is overall the most stable. The energies for the reconstructed structures are corrected by vacancy formation energies.[25] For unreconstructed adsorption, the atop site is the most stable in the $2\sqrt{3}$ phase, while the bridge site is most stable in the $\sqrt{13}$ phase, due to the 16.1° rotation of C_{60} between the two phases changing the inter-C_{60} interactions.

Phase	One-atom hole	Unreconstructed	Seven-atom hole
$2\sqrt{3}$	–4.79	–4.10 (atop)	–3.76
$\sqrt{13}$	–5.22	–4.59 (bridge)	–5.01

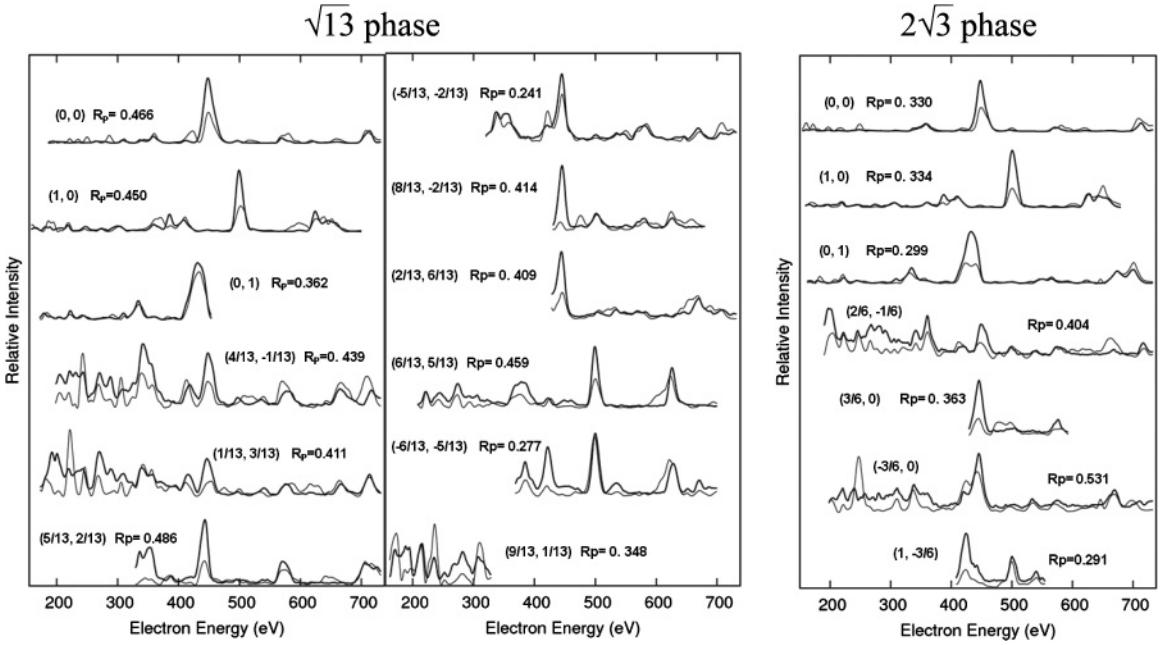

FIG. 2. Experimental (bold lines) and fitted I-V curves for the $\sqrt{13}$ (left) and $2\sqrt{3}$ (right) phases. Individual beam R factors are given. The overall R factor is 0.406 for the $\sqrt{13}$ phase and 0.370 for the $2\sqrt{3}$ phase.

proposed in a recent scanning tunneling microscopy study,[12] while providing much more information and reliability. In this structure, C_{60} sits on top of the Pt vacancy with hexagon down and forms six C-Pt covalent bonds with the six Pt atoms surrounding the vacancy. The C_{60} mirror planes are parallel to those of the Pt(111) surface. This adsorption configuration is very similar to that of C_{60} on Ag(111);[7] note that in the Pt and Ag cases, the results are almost insensitive to a 180° rotation of C_{60} around its axis perpendicular to the surface, which exchanges hexagonal and pentagonal faces around the molecular perimeter. Except for the one missing Pt atom, there is little displacement of the Pt atoms from their bulk positions. This is consistent with the x-ray-diffraction result for C_{60}/Pt(111) (Ref. 14) and similar to C_{60}/Ag(111),[7] but different from C_{60}/Cu(111).[4] The C-C bonds at the C_{60}-Pt interface (the bottom hexagon of C_{60}) are elongated by about 4%.

Carbon-60 on Pt(111) can form two phases due to a unique combination of factors, even while the local binding structure of C_{60} on Pt(111) remains the same: the particular value of the Pt lattice constant, 3.92 Å, coupled with a rotation by $30 - 13.9 = 16.1°$ of the superlattice cell from $(\sqrt{13} \times \sqrt{13})R13.9°$ to $(2\sqrt{3} \times 2\sqrt{3})R30°$ and the consequent relative rotation of the C_{60} molecules. These factors result in two structures that have nearly identical binding energies per surface area in spite of different inter-C_{60} geometries. Our detailed structural analysis shows that the $2\sqrt{3}$ phase can exist because the shortest C-C distance between two C_{60} molecules is reduced by only 0.1 Å relative to the $\sqrt{13}$ phase due to a better and denser packing [Figs. 1(e) and 1(f)], even though the supercell length (equal to the intermolecular center-to-center distance) is reduced by 0.39 Å (from 9.99 to 9.60 Å). In a pure C_{60} layer, the relative intermolecular orientation does not vary; however, it can change for C_{60} in the C_{60}/Pt combined system because the C_{60} molecules are fixed to orientations imposed by the Pt substrate via covalent bonding with Pt, while forming differently oriented superlattices in the $\sqrt{13}$ and $2\sqrt{3}$ phases, as seen in Figs. 1(c) and 1(d).

In fact, in hindsight, the similarity in the integer beams between the $\sqrt{13}$ and $2\sqrt{3}$ phases on Pt already indicates similar local adsorption structures. The two phases tend to coexist,[12,13] which agrees with the calculated adsorption energies for the one-atom hole structure (Table I) after considering the energy per surface area (a ratio of 13:12 between the two phases). Also note that forming more holes

TABLE II. Pendry R factors for the best-fit unreconstructed and reconstructed structures: The one-atom hole structure gives the overall best fit.

Phase	One-atom hole	Unreconstructed	Seven-atom hole
$2\sqrt{3}$	0.370	0.437 (hcp hollow)	0.719
$\sqrt{13}$	0.406	0.459 (atop)	0.539

TABLE III. Comparison of selected parameters for the C_{60}-Pt adsorption geometry from LEED and DFT results for the best-fit (one-atom hole) structures (in angstroms): Good agreement between LEED and DFT is obtained and both agree with a strong C-Pt covalent bond character (sum of covalent radii of Pt and C in sp^3 is 2.12 Å; C_{60}-to-Pt height is the spacing between nearest C and Pt layers).

Phase	Technique	C-Pt bond length	C_{60}-to-Pt height
$2\sqrt{3}$	LEED	2.15	1.67
$2\sqrt{3}$	DFT	2.08	1.63
$\sqrt{13}$	LEED	2.16	1.70
$\sqrt{13}$	DFT	2.09	1.65

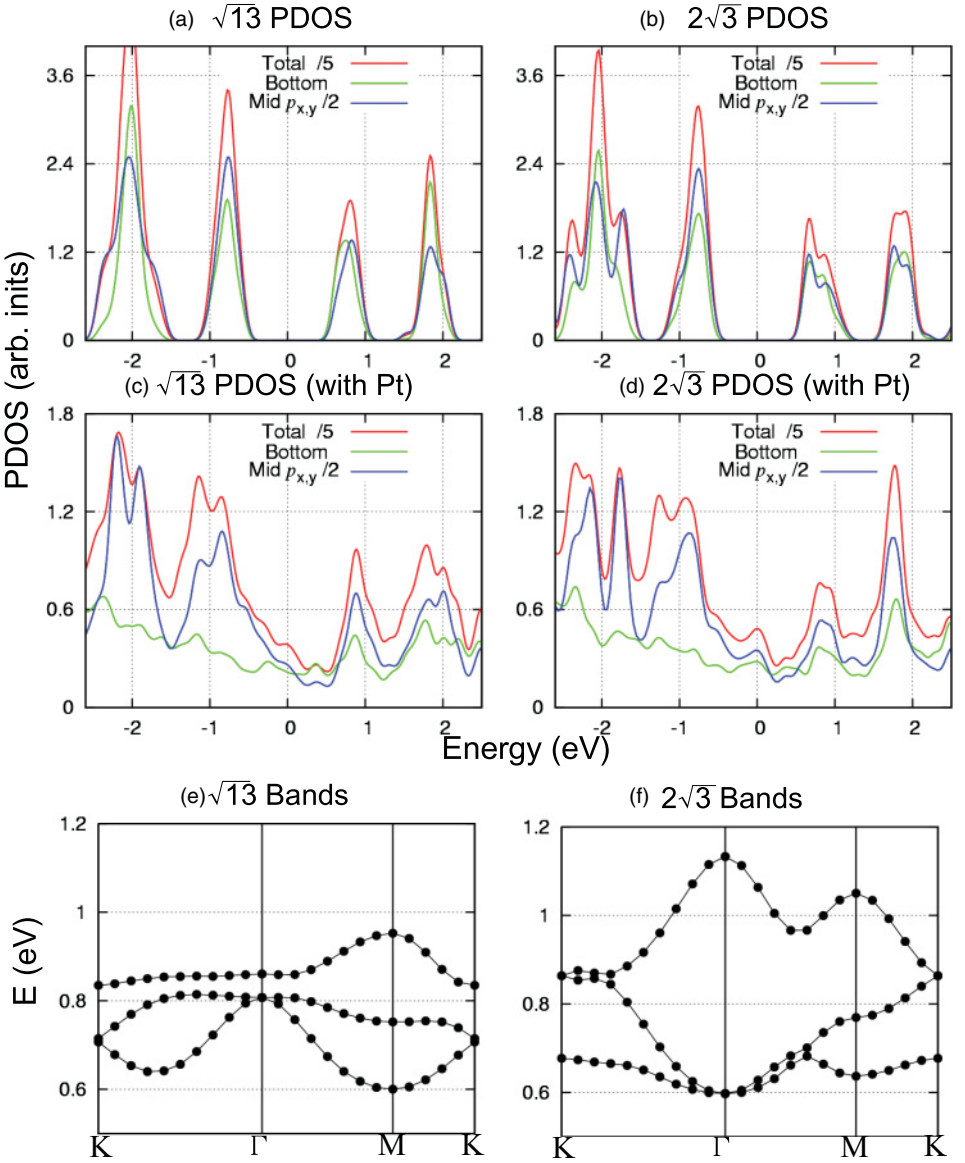

FIG. 3. (Color online) PDOS of C_{60} in the $\sqrt{13}$ and $2\sqrt{3}$ phases both (a) and (b) without and (c) and (d) with Pt substrate [red lines are the PDOS (divided by 5) of the complete C_{60}; green lines are the PDOS of the bottom 6 carbons that bind with Pt; blue lines are the PDOS (divided by 2) of the middle 18 carbons near the C_{60} equator, bordering neighboring molecules; and $p_{x,y}$ are p orbitals along the surface parallel directions]. A smaller ordinate range is used in the PDOS plots for C_{60} with Pt relative to those without Pt due to the larger peak broadening and hence smaller peak height with Pt. Also shown are the band structures of C_{60} LUMOs in the (e) $\sqrt{13}$ and (f) $2\sqrt{3}$ phases without Pt substrate (see the text).

is entropically favored at higher temperatures; so at higher temperatures the denser $2\sqrt{3}$ phase will be favored. This may be the reason why at higher deposition temperature (500 K) we can produce the $2\sqrt{3}$ phase alone (without $\sqrt{13}$). We suspect that, when depositing at 500 K, the one-atom hole reconstruction occurs immediately and we get the denser $2\sqrt{3}$ phase only, thanks to good parallel alignment of the molecules; note that the $\sqrt{13}$ unit-cell length fits the bulk C_{60} lattice better than the $2\sqrt{3}$ phase does. In contrast, after deposition at RT, the C_{60} molecules will initially have various orientations[12] so they cannot easily fit in the tighter $2\sqrt{3}$ unit cell [Figs. 1(e) and 1(f)]. It has moreover been observed that annealing at 500 K cannot partially change the $\sqrt{13}$ phase to the $2\sqrt{3}$ phase, while such changes may occur at even higher temperatures.[12]

Based on the determined geometric structures, we further study the electronic structures of C_{60} in these two phases by DFT calculations. To understand the effects of C_{60}-C_{60} and Pt-C_{60} interactions, Figs. 3(a)–3(d) show the projected density of states (PDOS) for the two phases both without [Figs. 3(a) and 3(b)] and with [Figs. 3(c) and 3(d)] Pt substrate. Comparing Figs. 3(a) and 3(b) for the PDOS between the two phases without Pt, we observe that the differences between the inter-C_{60} interactions of the two phases are reflected in differences in the peak shapes, including different peak broadening and splitting. These differences are due to the different inter-C_{60} orientations and distances, especially near the C_{60} "equator" (blue lines in the plots). Comparing Fig. 3(a) to 3(c) [and Fig. 3(b) to 3(d)] for the PDOS without and with Pt, we can see that the PDOS is also considerably affected by the Pt-C_{60} interactions: The peaks are broadened and split (or partially merged in the case of the unoccupied states in the $2\sqrt{3}$ phase). The peak positions also shift slightly. Thus the inter-C_{60} interactions change the peak shape, including broadening and splitting; these changes are enhanced by Pt-C_{60} interactions. The band splitting induced by Pt-C_{60} interactions is also observed in the projected band structure plots for the combined C_{60}/Pt system.[25] The strength of the C_{60}-Pt interactions is shown most clearly through the broadening of the bottom carbon PDOS (green lines). The covalent interactions result mainly in orbital renormalization,

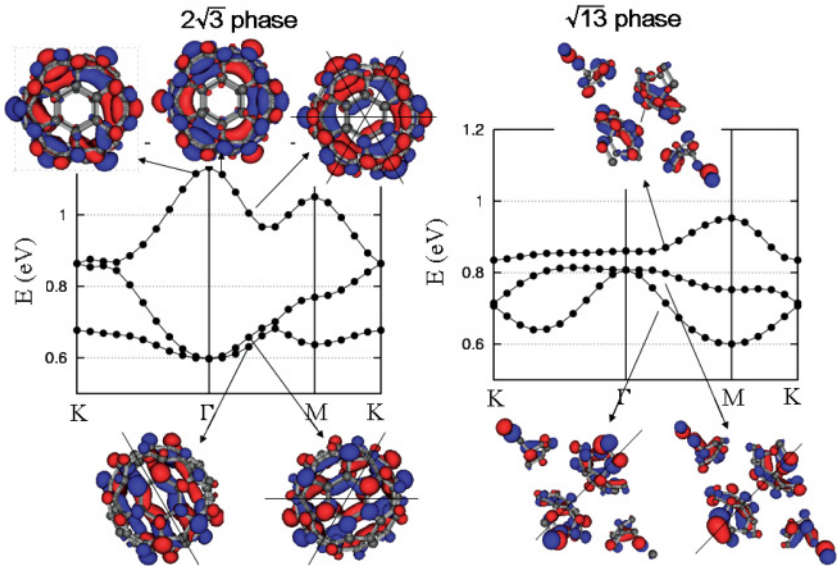

FIG. 4. (Color online) C_{60} LUMO wave function plots at several special K points (indicated by arrows) for C_{60} in the $2\sqrt{3}$ (left) and $\sqrt{13}$ (right) phases; the lines across C_{60} denote nearest inter-C_{60} directions.

but no significant energy shift and hence very small charge transfer: The Bader charge analysis[26] shows that the charge transfer is small and similar for both phases, ∼0.25 electrons transferred from the Pt surface to each C_{60}; this contrasts with a charge transfer of about 3 electrons in the C_{60}/Cu(111) system,[4] which undergoes a stronger metal reconstruction with 7 missing Cu atoms per molecule. Furthermore, the strong Pt-C_{60} interactions turn the C_{60} monolayer into a metal (states appear just below the Fermi level); also our simulated PDOS features using our reconstructed model fit the experimental spectroscopic data (ultraviolet photoemission spectroscopy and metastable atom electron spectroscopy data in Ref. 15) better than with the unreconstructed model adopted in that study.

For the lowest unoccupied molecular orbitals (LUMOs) of C_{60}, the effects of the Pt-C_{60} interactions on the PDOS are smaller than for other orbitals in the PDOS plots. Thus it is useful to compare the band structures of the C_{60} LUMOs to evaluate the effects of inter-C_{60} interactions. We choose to show the band structures of the C_{60} LUMOs because they would be closest to the Fermi level on metal surfaces subject to charge transfer that might be due, for example, to other adsorbates, in particular when doped with alkali-metal atoms.[2,5] The LUMOs consist mainly of p orbitals pointing radially at each carbon atom, hence they are sensitive to the C_{60} orientation.[2,6] Figures 3(e) and 3(f) show the band structures of the C_{60} LUMOs in the two phases; note that the directions in reciprocal space differ by about $30 - 13.9 = 16.1^\circ$ between Figs. 3(e) and 3(f) due to the different orientations of the $\sqrt{13}$ and $2\sqrt{3}$ unit cells relative to the orientation of the C_{60} and the Pt(111) lattice, i.e., these are cuts in slightly different directions of reciprocal space. The band dispersions and bandwidths are very different for the two phases. Two key features are observed: (i) a smaller bandwidth for the $\sqrt{13}$ phase than for the $2\sqrt{3}$ phase and (ii) the dispersion in the Γ-M direction is out of phase. This means that for the $2\sqrt{3}$ phase the lower two bands disperse upward and the upper band disperses downward from Γ, while for the $\sqrt{13}$ phase the lower two bands disperse downward and the upper band disperses upward from Γ. Feature (i) can be explained by the different C_{60}-C_{60} distances in the two structures: smaller distances result in stronger inter-C_{60} interactions and hence larger bandwidth, and vice versa. Feature (ii) is due to the different relative inter-C_{60} orientations between the two phases, which causes the intermolecular interaction to become out of phase between the bands that exhibit upward vs downward dispersions (this is illustrated in the wave-function plots in Fig. 4): For the upward dispersion the nearest interacting C atoms on neighboring molecules exhibit LUMO wave functions with the same phase, while for the downward dispersion the LUMO wave functions have opposite phases.

Figure 4 shows the C_{60} LUMO wave-function plots at several special K points for C_{60} in the two phases. At the nearest C_{60}-C_{60} approach, if the molecular orbitals (MOs) have different signs, the energy band will disperse downward (for example, for the upper band in the $2\sqrt{3}$ phase); if the MOs have the same sign, the energy band will disperse upward (for example, for the upper band in the $\sqrt{13}$ phase). However, it must be emphasized that the details can be more complicated because (i) the contribution may not come from the nearest carbons on neighboring C_{60} molecules if there is no suitable wave function, but may be from more distant carbons; and (ii) C_{60} has six (more precisely three) different nearest-neighbor C_{60} molecules. Different nearest neighbors may have different behaviors while the final band dispersion is an overall combined effect.

Finally, it should be noted that the dependence of the band structure for C_{60} upon relative orientation of neighboring molecules that has been reported in Ref. 2 is based on a comparison of C_{60} on the Ag(111) and Ag(100) surfaces. Since these two systems have quite different C_{60}-metal interfaces, the origin of the band structure differences is not as clearcut as for the present two structures on Pt(111). Indeed, our DFT results on Pt(111) prove that large band-structure changes also occur for C_{60} in essentially identical local adsorption geometries upon relative molecular reorientation; therefore, these changes in the C_{60} electronic structures must result predominantly from the differences in inter-C_{60} interactions. Note that in Figs. 3(e) and 3(f) we show the energy bands for C_{60} without Pt substrate in the two phases (since the band plot becomes very crowded

for the full system; plots for the C_{60}/Pt composite system are provided in Ref. 25).

IV. CONCLUSION

We have prepared the isolated $\sqrt{13}$ and $2\sqrt{3}$ phases of C_{60} monolayers on Pt(111) without mixing, determined the monolayer structures in both phases by combined dynamic LEED and DFT calculations, and demonstrated significant differences in the electronic structures of C_{60} monolayers in these two phases by DFT calculations. The binding of C_{60} on Pt in the two phases changes the relative inter-C_{60} orientations and hence the electronic properties are changed: Small differences in inter-C_{60} orientations have a relatively large effect on the electronic properties because of the high angular momentum of C_{60} orbitals. One may therefore also expect electronic structure differences for C_{60} monolayers on other surfaces with different phases, such as for C_{60} on Ag(100) (Refs. 2, 10, and 11) and on Al(111),[9] and more generally with other adsorbates and substrates. Thus our results demonstrate a way to structurally tune electronic properties for molecular films or junctions composed of the same materials. These results suggest that parallel studies of other properties, such as electronic transport and magnetism, in these systems with and without further doping would be highly desirable.

ACKNOWLEDGMENTS

This work was supported in part by Hong Kong RGC Grant No. CityU 102707 and the CityU Centre for Applied Computing and Interactive Media.

[1]W. L. Yang *et al.*, Science **300**, 303 (2003).
[2]V. Brouet, W. L. Yang, X. J. Zhou, H. J. Choi, S. G. Louie, M. L. Cohen, A. Goldoni, F. Parmigiani, Z. Hussain, and Z. X. Shen, Phys. Rev. Lett. **93**, 197601 (2004).
[3]V. Brouet, W. L. Yang, X. J. Zhou, H. J. Choi, S. G. Louie, M. L. Cohen, A. Goldoni, F. Parmigiani, Z. Hussain, and Z. X. Shen, Phys. Rev. Lett. **95**, 099903(E) (2005).
[4]W. W. Pai *et al.*, Phys. Rev. Lett. **104**, 036103 (2010); G. Xu, X. Q. Shi, M. A. Van Hove, and W. W. Pai (unpublished).
[5]Y.-M. Byun, H. J. Choi, S. G. Louie, and M. L. Cohen, Phys. Rev. B **77**, 115418 (2008).
[6]N. Laouini, O. K. Andersen, and O. Gunnarsson, Phys. Rev. B **51**, 17446 (1995).
[7]H. I. Li *et al.*, Phys. Rev. Lett. **103**, 056101 (2009).
[8]G. Schull and R. Berndt, Phys. Rev. Lett. **99**, 226105 (2007).
[9]M. Stengel, A. DeVita, and A. Baldereschi, Phys. Rev. Lett. **91**, 166101 (2003).
[10]W. W. Pai and C.-L. Hsu, Phys. Rev. B **68**, 121403(R) (2003).
[11]C.-L. Hsu and W. W. Pai, Phys. Rev. B **68**, 245414 (2003).
[12]C. D. Liu, Z. H. Qin, J. Chen, Q. M. Guo, Y. H. Yu, and G. Y. Cao, J. Chem. Phys. **134**, 044707 (2011).
[13]M. Pedio, K. Hevesi, N. Zema, M. Capozi, P. Perfetti, R. Gouttebaron, J.-J. Pireaux, R. Caudano, and P. Rudolf, Surf. Sci. **437**, 249 (1999).
[14]R. Felici, M. Pedio, F. Borgatti, S. Iannotta, M. Capozi, G. Ciullo, and A. Stierle, Nature Mater. **4**, 688 (2005).
[15]M. Sogo, Y. Sakamoto, M. Aoki, S. Masuda, S. Yanagisawa, and Y. Morikawa, J. Phys. Chem. C **114**, 3504 (2010).
[16]M. Kiguchi, Appl. Phys. Lett. **95**, 073301 (2009).
[17]M. S. Altman, J. Phys. Condens. Matter **22**, 084017 (2010).
[18]M. A. Van Hove, W. Moritz, H. Over, P. J. Rous, A. Wander, A. Barbieri, N. Materer, U. Starke, and G. A. Somorjai, Surf. Sci. Rep. **19**, 191 (1993).
[19]J. Rundgren, Phys. Rev. B **68**, 125405 (2003).
[20]N. Materer, U. Starke, A. Barbieri, R. Döll, K. Heinz, M. A. Van Hove, and G. A. Somorjai, Surf. Sci. **325**, 207 (1995).
[21]G. Kresse and J. Furthmüller, Comput. Mater. Sci. **6**, 15 (1996).
[22]D. M. Ceperley and B. J. Alder, Phys. Rev. Lett. **45**, 566 (1980).
[23]L.-L. Wang and H.-P. Cheng, Phys. Rev. B **69**, 165417 (2004).
[24]G. Kresse and D. Joubert, Phys. Rev. B **59**, 1758 (1999).
[25]See Supplemental Material at http://link.aps.org/supplemental/10.1103/PhysRevB.84.235406 for the calculations of vacancy formation energies and projected bands and for atomic coordinates and LEED *I*-*V* data.
[26]W. Tang, E. Sanville, and G. Henkelman, J. Phys. Condens. Matter, **21**, 084204 (2009).